DG SOLVER FOR THE SIMULATION OF SIMPLIFIED ELASTIC WAVES IN TWO-DIMENSIONAL PIECEWISE HOMOGENEOUS MEDIA

J. Hozman[*], *J. Bradáč*[†], *J. Kovanda*[‡]

Abstract: The theory of elasticity is a very important discipline which has a lot of applications in science and engineering. In this paper we are interested in elastic materials with different properties between interfaces implicated the discontinuous coefficients in the governing elasticity equations. The main aim is to develop a practical numerical scheme for modeling the behaviour of a simplified piecewise homogeneous medium subjected to an external action in 2D domains. Therefore, the discontinuous Galerkin method is used for the simulation of elastic waves in such elastic materials. The special attention is also paid to treatment of boundary and interface conditions. For the treatment of the time dependency the implicit Euler method is employed. Moreover, the limiting procedure is incorporated in the resulting numerical scheme in order to overcome nonphysical spurious overshoots and undershoots in the vicinity of discontinuities in discrete solutions. Finally, we present computational results for two-component material, representing a planar elastic body subjected to a mechanical hit or mechanical loading.

Key words: *elastic wave equation, piecewise homogeneous medium, discontinuous Galerkin method, interface conditions, implicit Euler method, limiting*

Received: December 15, 2015 **DOI:** 10.14311/NNW.2017.27.021
Revised and accepted: August 30, 2017

1. Introduction

Solid materials, that should meet the required elastic properties needed for their purpose, are common in a wide range of scientific disciplines dealing with material engineering. This elastic ability can be described as a preservation of the original shape and material properties after the removal of the acting force, which induces a propagation of elastic waves. An elastic wave is a type of mechanical wave travelling

[*]Jiří Hozman; Technical University of Liberec, Faculty of Science, Humanities and Education, Studentská 2, CZ-461 17 Liberec, Czech Republic, E-mail: jiri.hozman@tul.cz

[†]Josef Bradáč; ŠKODA AUTO University, Na Karmeli 1457, CZ-293 01 Mladá Boleslav, Czech Republic, E-mail: josef.bradac@savs.cz

[‡]Jan Kovanda; University of West Bohemia, Faculty of Mechanical Engineering – Regional Technological Institute, Univerzitní 8, CZ-306 14 Plzeň, Czech Republic, E-mail: kovanda@rti.zcu.cz

through a given medium, or on its surface, without causing permanent structural changes. It is typically identified by a disturbance described by a distortion or displacement, for a survey see [5, 10].

The real-world problems are defined in 3D and treated with heterogeneous medium, in general. Their detailed analysis and solving are often difficult due to the complexity of the whole problem. Therefore, various simplifications and idealization of original models are selected under the fulfillment of additional assumptions.

If the 3D problem possesses at least one axial symmetry, the model can be easily reformulated into two dimensions. Furthermore, to simplify the structure of heterogeneous solids, it is possible to consider a piecewise homogeneous elastic medium including sharp interfaces, where the different translation properties are modeled by piecewise constant functions specifying the speed of the wave propagation in this medium.

Since the construction of analytic solutions of such problems is limited by their complexity, the article focuses only on numerical treatment to their solving. There are several numerical techniques dealing with the similar problem using finite differences or finite elements, for recent studies we refer the reader to [1, 11, 15]. An alternative approach, which credibly reflects discontinuities in material parameters, is a discontinuous Galerkin (DG) method based on piecewise polynomial but discontinuous approximations, for the detailed description see [2, 3, 7, 12].

The paper presents the DG solver supplemented with an automatic limiting (cf. [4]) and the special attention is also paid to the treatment of a numerical flux, interface and boundary conditions. Therefore, the resulting scheme enables to better resolve the behaviour of solutions in the neighbourhood of interfaces. From the practical point of view, two types of numerical experiments are mentioned in the dimensionless scale, both represent the different ways of a mechanical interaction with a planar elastic body consisting of two-component material.

2. Problem statement

In this section, we present the fundamental equations of the theory of linearized elasticity and introduce the equation, which governs the propagation of mechanical waves in the simplified elastic materials. The second part is devoted to the description of a medium consisting of different components.

2.1 Governing equations

The relative geometric deformation of the solid is called a strain and forces that occur in the solid are described as stresses. The linear theory of elasticity represented by the resulting system can also model mechanical properties in an elastic structure. Using this theory several phenomena, such as a propagation of mechanical shock waves in these media, can be simulated.

We consider the following equation

$$\rho \frac{\partial^2 \boldsymbol{u}}{\partial t^2} - \operatorname{div}(\mathcal{T}(\boldsymbol{u})) = 0 \quad \text{in } \Omega \times (0, T), \tag{1}$$

where the bounded domain $\Omega \subset \mathbb{R}^2$ is occupied by an elastic medium with the density $\rho(\boldsymbol{x})$ depending on the spatial variable $\boldsymbol{x} = [x, y] \in \Omega$, the vector field $\boldsymbol{u} = (u(\boldsymbol{x}, t), v(\boldsymbol{x}, t))^{\mathrm{T}}$ denotes the two-dimensional displacement and $\mathcal{T}(\boldsymbol{u}) = (\tau_{ij}(\boldsymbol{u}))_{i,j=1}^2$ is the stress tensor, whose components are given by generalized Hooke's law. Let us note that its diagonal components present normal stresses and the other components present shear stresses.

Furthermore, we can think of this system as a particular simplified model that describes propagation of elastic waves. In a solid, an elastic wave is composed of longitudinal and transversal waves. If we neglect the effect of transversal waves (i.e. $\tau_{12} = \tau_{21} = 0$) and assume that the stress is the same in all directions (i.e. $\tau_{11} = \tau_{22}$), the generalized Hooke's law can be reduced to a simple linear constitutive relation given by

$$\sigma = E \operatorname{tr}(\varepsilon(\boldsymbol{u})) = E(\varepsilon_{11}(\boldsymbol{u}) + \varepsilon_{22}(\boldsymbol{u})),$$

where σ is the stress, E the Young modulus and $\varepsilon(\boldsymbol{u}) = (\varepsilon_{ij}(\boldsymbol{u}))_{i,j=1}^2$ the linearized strain tensor, defined by

$$\varepsilon(\boldsymbol{u}) = \begin{pmatrix} \frac{\partial u}{\partial x} & \frac{1}{2}\left(\frac{\partial u}{\partial y} + \frac{\partial v}{\partial x}\right) \\ \frac{1}{2}\left(\frac{\partial u}{\partial y} + \frac{\partial v}{\partial x}\right) & \frac{\partial v}{\partial y} \end{pmatrix}.$$

Thus, the stress tensor can be written in the following matrix form

$$\mathcal{T}(\boldsymbol{u}) = \begin{pmatrix} \sigma & 0 \\ 0 & \sigma \end{pmatrix} = E \begin{pmatrix} \frac{\partial u}{\partial x} + \frac{\partial v}{\partial y} & 0 \\ 0 & \frac{\partial u}{\partial x} + \frac{\partial v}{\partial y} \end{pmatrix}. \tag{2}$$

Let $\epsilon = \varepsilon_{11} + \varepsilon_{22}$ denote the first strain invariant, usually called as the (two-dimensional) volumetric strain. Then the propagation of mechanical waves in the elastic medium can be modeled by the system resulting from Eqns. (1) and (2), written in scalar form

$$\begin{aligned} \rho \frac{\partial^2 u}{\partial t^2} - \frac{\partial \sigma}{\partial x} &= 0, \\ \rho \frac{\partial^2 v}{\partial t^2} - \frac{\partial \sigma}{\partial y} &= 0, \\ \epsilon - \frac{\partial u}{\partial x} - \frac{\partial v}{\partial y} &= 0. \end{aligned} \tag{3}$$

It is also possible and usual to reduce the second order equations to the first order system of hyperbolic equations with canonical form. Indeed by introducing the wave speed $c = \sqrt{E/\rho}$ and setting

$$\boldsymbol{w} = (w_1, w_2, w_3)^{\mathrm{T}} \equiv \left(\rho \frac{\partial u}{\partial t}, \rho \frac{\partial v}{\partial t}, \sigma\right)^{\mathrm{T}}$$

the system in Eq. (3) leads to

$$\frac{\partial \boldsymbol{w}}{\partial t} + \frac{\partial \boldsymbol{f}(\boldsymbol{w})}{\partial x} + \frac{\partial \boldsymbol{g}(\boldsymbol{w})}{\partial y} = 0 \quad \text{in } \Omega \times (0, T), \tag{4}$$

where the vector functions

$$\boldsymbol{f}(\boldsymbol{w}) = \left(-w_3, 0, -c^2 w_1\right)^{\mathrm{T}} \quad \text{and} \quad \boldsymbol{g}(\boldsymbol{w}) = \left(0, -w_3, -c^2 w_2\right)^{\mathrm{T}}$$

are the physical fluxes in x- and y-direction, respectively. Let us mention that the state vector $\boldsymbol{w}$ consists of two components of momentum and the third one is the stress. Moreover, notice that the third equation of the system (4) corresponds to the time derivative of the third relation in Eq. (3) multiplied by E.

Finally, in order to obtain the correctly defined initial-boundary value problem, the system (4) is closed by the vector of initial conditions

$$\boldsymbol{w}^0 = (w_1^0(\boldsymbol{x}), w_2^0(\boldsymbol{x}), w_3^0(\boldsymbol{x}))^{\mathrm{T}} \quad \text{at } t = 0$$

and the boundary conditions prescribed on the boundary $\partial\Omega$. The choice of boundary conditions is always a delicate issue, and thus in this case, we simply write them as $B(\boldsymbol{w}) = 0$ on $\partial\Omega$.

2.2 Description of a piecewise homogeneous medium

In what follows, we focus on the description of the computational domain Ω occupied by the piecewise homogeneous elastic medium consisting of two subdomains Ω_A, Ω_B with the common interface Γ_I. The setting of the whole domain is illustrated in Fig. 1, obviously, $\Omega = \Omega_A \cup \Omega_B \cup \Gamma_I$.

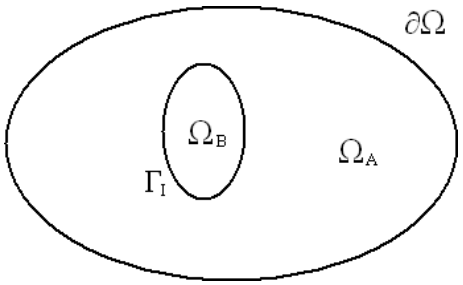

Fig. 1 *The structure of the domain Ω, its subdomains and the position of the interface and boundary.*

On the interface Γ_I between subdomains Ω_A and Ω_B, displacements and normal components of forces should be balanced, i.e.,

$$\boldsymbol{u}_B - \boldsymbol{u}_A = 0, \tag{5}$$

$$\mathcal{T}(\boldsymbol{u}_B)\boldsymbol{n}_B + \mathcal{T}(\boldsymbol{u}_A)\boldsymbol{n}_A = 0, \tag{6}$$

where $\boldsymbol{u}_A = \boldsymbol{u}|_{\Omega_A}$ and $\boldsymbol{u}_B = \boldsymbol{u}|_{\Omega_B}$. The symbols $\boldsymbol{n}_A$ and $\boldsymbol{n}_B$ stand for the unit outer normals to Γ_I with respect to Ω_A and Ω_B, respectively.

Since the outward normal $\boldsymbol{n}_A$ is the inward normal for Ω_B, i.e. $\boldsymbol{n}_A = -\boldsymbol{n}_B$, and using Eq. (2), the interface conditions (5) and (6) can be rewritten in scalar form

$$u_B = u_A, \qquad v_B = v_A, \qquad \sigma_B = \sigma_A, \tag{7}$$

which means that the elastic material has no fracture in the discontinuity setting i.e., the displacements and stresses are still continuous across the interface.

However, the discontinuities in the material coefficients often occur over the interface. In our case, for the piecewise homogeneous elastic medium with one interface, constitutive equations are determined with two parameters, density ρ and Young modulus E. So ρ and E are positive and across the interface Γ_I they are discontinuous. For simplicity, we assume that they are piecewise constant and given by

$$\rho(\boldsymbol{x}) = \begin{cases} \rho_A, & \boldsymbol{x} \in \Omega_A, \\ \rho_B, & \boldsymbol{x} \in \Omega_B, \end{cases} \qquad E(\boldsymbol{x}) = \begin{cases} E_A, & \boldsymbol{x} \in \Omega_A, \\ E_B, & \boldsymbol{x} \in \Omega_B, \end{cases} \tag{8}$$

where ρ_A, ρ_B and E_A, E_B are positive constants. In parallel to the definition (8), we obtain the different wave speeds in each subdomain, namely

$$c_A = \sqrt{E_A/\rho_A} \text{ in } \Omega_A \quad \text{and} \quad c_B = \sqrt{E_B/\rho_B} \text{ in } \Omega_B.$$

The description of the material properties via wave speeds enables us to easily formulate the problem in the dimensionless scale.

Finally, we can express the relations Eq. (7) in the state vector components as

$$\rho_A\,(w_1|_{\Omega_B}) = \rho_B\,(w_1|_{\Omega_A})\,,\ \rho_A\,(w_2|_{\Omega_B}) = \rho_B\,(w_2|_{\Omega_A})\,,\ w_3|_{\Omega_B} = w_3|_{\Omega_A} \text{ on } \Gamma_I, \tag{9}$$

where the first two relations in Eq. (9) are obtained by differentiating the corresponding equations in Eq. (7) with respect to time.

3. Discrete wave problem

In a wide class of problems resulting to a solution of partial differential equations, the DG method is rather popular. We start with a triangulation of the computational domain and define a finite dimensional space. Then we derive the DG formulation of the problem, construct the corresponding linear algebraic problem and end up with the numerical scheme. Special attention is also paid to the evaluation of the numerical flux on the boundary and interfaces. Moreover, an automatic limiting is incorporated to the resulting scheme.

3.1 Space semidiscretization

The standard DG method uses piecewise polynomial, generally discontinuous, approximation of the p-th order describing a global solution on the whole domain Ω. Therefore, the approximate solution $\boldsymbol{w}_h$ is sought in a finite dimensional space

$$\boldsymbol{S}_{hp} = [S_{hp}]^3, \quad \text{with} \quad S_{hp} = \{\varphi \in L^2(\Omega);\, \varphi|_K \in P_p(K)\ \forall\, K \in \mathcal{T}_h\},$$

where $\mathcal{T}_h$ is a partition of the closure of the computational domain $\overline{\Omega}$ into a finite number of closed elements K with mutually disjoint interiors such that $\Omega = \cup_{K\in\mathcal{T}_h} K$, h represents the mesh size and $P_p(K)$ denotes the space of all polynomials of order less or equal to p defined on K.

By $\mathcal{F}_h$ we denote the set of all open edges of all elements $K \in \mathcal{T}_h$. Further, the symbol $\mathcal{F}_h^I$ stands for the set of all $\Gamma \in \mathcal{F}_h$ that are contained in $\Omega\backslash\Gamma_I$ (interior),

the symbol $\mathcal{F}_h^T$ for the set of all $\Gamma \in \mathcal{F}_h$ such that $\Gamma \subset \Gamma_I$ (interface) and the symbol $\mathcal{F}_h^B$ for the set of all $\Gamma \in \mathcal{F}_h$ such that $\Gamma \subset \partial\Omega$ (boundary). Obviously, $\mathcal{F}_h = \mathcal{F}_h^I \cup \mathcal{F}_h^T \cup \mathcal{F}_h^B$. Finally, for each $\Gamma \in \mathcal{F}_h$, we assign the unit normal vector $\boldsymbol{n}_\Gamma$. We assume that $\boldsymbol{n}_\Gamma$, $\Gamma \subset \partial\Omega$, has the same orientation as the outer normal of $\partial\Omega$. For $\boldsymbol{n}_\Gamma$, $\Gamma \in \mathcal{F}_h^I$, the orientation is arbitrary but fixed for each edge.

For each $\Gamma \in \mathcal{F}_h^I$ there exist two elements K_L, $K_R \in \mathcal{T}_h$ such that $\Gamma \subset K_L \cap K_R$. We use a convention that K_R lies in the direction of $\boldsymbol{n}_\Gamma$ and K_L in the opposite direction of $\boldsymbol{n}_\Gamma$. Since a function $\boldsymbol{\varphi} \in \boldsymbol{S}_{hp}$ is, in general, discontinuous on edges $\Gamma \in \mathcal{F}_h^I$, we define $\boldsymbol{\varphi}|_\Gamma^{(L)}$ and $\boldsymbol{\varphi}|_\Gamma^{(R)}$ as the traces of $\boldsymbol{\varphi}|_{K_L}$ and $\boldsymbol{\varphi}|_{K_R}$ on edge Γ, respectively. These traces are different in general and lead to the definition of jump and average, i.e.,

$$[\boldsymbol{\varphi}]_\Gamma = \boldsymbol{\varphi}_\Gamma^{(L)} - \boldsymbol{\varphi}_\Gamma^{(R)}, \qquad \langle\boldsymbol{\varphi}\rangle_\Gamma = \frac{1}{2}\left(\boldsymbol{\varphi}_\Gamma^{(L)} + \boldsymbol{\varphi}_\Gamma^{(R)}\right).$$

For $\Gamma \in \partial\Omega$ there exists an element $K_L \in \mathcal{T}_h$ such that $\Gamma \subset K_L \cap \partial\Omega$. Then for $\boldsymbol{\varphi} \in S_{h\mathfrak{p}}$, we put $\langle\boldsymbol{\varphi}\rangle_\Gamma = [\boldsymbol{\varphi}]_\Gamma = \boldsymbol{\varphi}|_\Gamma^{(L)}$.

In order to obtain a semi-discrete formulation, we follow the concept from [8] and multiply the corresponding original Eq. (4) by a test function $\boldsymbol{\varphi}_h \in \boldsymbol{S}_{hp}$, integrate over an element $K \in \mathcal{T}_h$ and apply Green's theorem. Further we sum over all $K \in \mathcal{T}_h$ and introduce the numerical flux based on upwinding in a discretization of the physical fluxes. In this way we get the following form:

$$\begin{aligned}
\boldsymbol{b}_h(\boldsymbol{w}_h(t), \boldsymbol{\varphi}_h) \;=\; & -\sum_{K\in\mathcal{T}_h}\int_K \boldsymbol{f}(\boldsymbol{w}_h)\cdot\frac{\partial\boldsymbol{\varphi}_h}{\partial x}\,\mathrm{d}\boldsymbol{x} - \sum_{K\in\mathcal{T}_h}\int_K \boldsymbol{g}(\boldsymbol{w}_h)\cdot\frac{\partial\boldsymbol{\varphi}_h}{\partial y}\,\mathrm{d}\boldsymbol{x} \\
& + \sum_{\Gamma\in\mathcal{F}_h^I}\int_\Gamma I\!H\left(\boldsymbol{w}_h^{(L)}, \boldsymbol{w}_h^{(R)}, \boldsymbol{n}_\Gamma\right)\cdot[\boldsymbol{\varphi}_h]_\Gamma\,\mathrm{d}S \\
& + \sum_{\Gamma\in\mathcal{F}_h^T}\int_\Gamma I\!H\left(\boldsymbol{w}_h^{(L)}, \boldsymbol{w}_h^{(A)}, \boldsymbol{n}_B\right)\cdot\boldsymbol{\varphi}_h^{(L)}\,\mathrm{d}S \\
& + \sum_{\Gamma\in\mathcal{F}_h^T}\int_\Gamma I\!H\left(\boldsymbol{w}_h^{(R)}, \boldsymbol{w}_h^{(B)}, \boldsymbol{n}_A\right)\cdot\boldsymbol{\varphi}_h^{(R)}\,\mathrm{d}S \\
& + \sum_{\Gamma\in\mathcal{F}_h^B}\int_\Gamma I\!H\left(\boldsymbol{w}_h^{(L)}, \boldsymbol{w}_h^{(E)}, \boldsymbol{n}_\Gamma\right)\cdot\boldsymbol{\varphi}_h^{(L)}\,\mathrm{d}S
\end{aligned} \tag{10}$$

where values of states $\boldsymbol{w}_h^{(A)}$, $\boldsymbol{w}_h^{(B)}$ are given by interface conditions and $\boldsymbol{w}_h^{(E)}$ by boundary conditions, see Sec. 3.2.

The form $\boldsymbol{b}_h$ is defined with the aid of a numerical flux $I\!H$, which is required to be consistent with the fluxes $\boldsymbol{f}$ and $\boldsymbol{g}$, i.e., $I\!H(\boldsymbol{w}, \boldsymbol{w}, \boldsymbol{n}) = \boldsymbol{f}(\boldsymbol{w})n_1 + \boldsymbol{g}(\boldsymbol{w})n_2$ ($\boldsymbol{n} = (n_1, n_2)^{\mathrm{T}}, |\boldsymbol{n}| = 1$); conservative, i.e., $I\!H(\boldsymbol{w}, \boldsymbol{z}, \boldsymbol{n}) = -I\!H(\boldsymbol{z}, \boldsymbol{w}, -\boldsymbol{n})$; and locally Lipschitz-continuous. Since the problem in Eq. (4) is linear with respect to the state vector, all terms in Eq. (10) should be expressed linearly in the variable $\boldsymbol{w}_h$.

Firstly, the physical fluxes in the volume integrals in Eq. (10) can be rewritten as $\boldsymbol{f}(\boldsymbol{w}) = \mathbf{A}(\boldsymbol{x})\boldsymbol{w}$ and $\boldsymbol{g}(\boldsymbol{w}) = \mathbf{B}(\boldsymbol{x})\boldsymbol{w}$ with matrices

$$\mathbf{A}(\boldsymbol{x}) = \begin{pmatrix} 0 & 0 & -1 \\ 0 & 0 & 0 \\ -c^2 & 0 & 0 \end{pmatrix}, \quad \mathbf{B}(\boldsymbol{x}) = \begin{pmatrix} 0 & 0 & 0 \\ 0 & 0 & -1 \\ 0 & -c^2 & 0 \end{pmatrix}. \tag{11}$$

One can easily observe that matrices in Eq. (11) are actually Jacobi matrices of the corresponding mappings.

Secondly, we choose the Vijayasundaram numerical flux (analogously to [8]) preserving the linearity of $\boldsymbol{w}_h$ in the path integrals in Eq. (10). Thus, taking into account the definition of aforementioned fluxes, we define the matrix

$$\mathbf{P}(\boldsymbol{n}) = \frac{D\boldsymbol{f}(\boldsymbol{w})}{D\boldsymbol{w}} n_1 + \frac{D\boldsymbol{g}(\boldsymbol{w})}{D\boldsymbol{w}} n_2 = \mathbf{A}(\boldsymbol{x}) n_1 + \mathbf{B}(\boldsymbol{x}) n_2, \ \boldsymbol{n} = (n_1, n_2)^{\mathrm{T}}, |\boldsymbol{n}| = 1. \quad (12)$$

The matrix $\mathbf{P}$ is independent of $\boldsymbol{w}$ and diagonalizable, i.e. there exist matrices $\boldsymbol{\Lambda}$ and $\mathbf{S}$ such that $\mathbf{P}(\boldsymbol{n}) = \mathbf{S}(\boldsymbol{n})\boldsymbol{\Lambda}\mathbf{S}^{-1}(\boldsymbol{n})$ and $\boldsymbol{\Lambda} = \mathrm{diag}(\lambda_1, \lambda_2, \lambda_3)$, where λ_i are eigenvalues of the matrix $\mathbf{P}$ and columns of $\mathbf{S}$ are the corresponding eigenvectors. Easy calculation leads to $\lambda_1 = -c$, $\lambda_2 = c$ and $\lambda_3 = 0$ with the following eigenvectors:

$$\mathbf{v}_{\lambda_1}(\boldsymbol{n}) = \left(\frac{n_1}{c}, \frac{n_2}{c}, 1\right)^{\mathrm{T}}, \quad \mathbf{v}_{\lambda_2}(\boldsymbol{n}) = \left(-\frac{n_1}{c}, -\frac{n_2}{c}, 1\right)^{\mathrm{T}}, \quad \mathbf{v}_{\lambda_3}(\boldsymbol{n}) = \left(-\frac{n_2}{n_1}, 1, 0\right)^{\mathrm{T}}.$$

Now we define the positive and negative parts of the matrix $\mathbf{P}$ by

$$\mathbf{P}^+(\boldsymbol{n}) = \mathbf{S}(\boldsymbol{n})\,\mathrm{diag}(0, c, 0)\,\mathbf{S}^{-1}(\boldsymbol{n}), \quad \mathbf{P}^-(\boldsymbol{n}) = \mathbf{S}(\boldsymbol{n})\,\mathrm{diag}(-c, 0, 0)\,\mathbf{S}^{-1}(\boldsymbol{n}). \quad (13)$$

After short manipulation with relations from Eq. (13), we obtain

$$\mathbf{P}^+(\boldsymbol{n}) = \frac{1}{2}\begin{pmatrix} cn_1^2 & cn_1n_2 & -n_1 \\ cn_1n_2 & cn_2^2 & -n_2 \\ -c^2n_1 & -c^2n_2 & c \end{pmatrix}, \quad (14)$$

$$\mathbf{P}^-(\boldsymbol{n}) = \frac{1}{2}\begin{pmatrix} -cn_1^2 & -cn_1n_2 & -n_1 \\ -cn_1n_2 & -cn_2^2 & -n_2 \\ -c^2n_1 & -c^2n_2 & -c \end{pmatrix}, \quad (15)$$

and the Vijayasundaram numerical flux reads

$$\mathit{I\!H}_V\left(\boldsymbol{w}_h^{(L)}, \boldsymbol{w}_h^{(R)}, \boldsymbol{n}_\Gamma\right) = \mathbf{P}^+(\boldsymbol{n})\,\boldsymbol{w}_h^{(L)} + \mathbf{P}^-(\boldsymbol{n})\,\boldsymbol{w}_h^{(R)}. \quad (16)$$

The remaining treatment of interface and boundary states in the numerical flux (16) will be discussed in more details later in the forthcoming section.

Finally, the semidiscrete solution is defined as $\boldsymbol{w}_h(t) \in \boldsymbol{S}_{hp}$ such that

$$\frac{\mathrm{d}}{\mathrm{d}t}\left(\boldsymbol{w}_h(t), \boldsymbol{\varphi}_h\right) + \boldsymbol{b}_h(\boldsymbol{w}_h(t), \boldsymbol{\varphi}_h) = 0 \quad \forall\, \boldsymbol{\varphi}_h \in \boldsymbol{S}_{hp}, \forall\, t \in (0, T), \quad (17)$$

where $(\cdot, \cdot)$ denotes the inner product in $[L^2(\Omega)]^3$ and $\boldsymbol{w}_h(0) = \boldsymbol{w}_h^0$ is an approximation of the initial state $\boldsymbol{w}^0$.

3.2 Treatment of interface and boundary conditions

If $\Gamma \in \mathcal{F}_h^T$, it is necessary to specify the states $\boldsymbol{w}_h^{(A)}$, $\boldsymbol{w}_h^{(B)}$ appearing in the numerical flux $\mathit{I\!H}$ in Eq. (10). According to the coupling conditions (9) it holds

$$\boldsymbol{w}_h^{(A)} = \left(\frac{\rho_A}{\rho_B}\, w_1^{(L)}, \frac{\rho_A}{\rho_B}\, w_2^{(L)}, w_3^{(L)}\right)^{\mathrm{T}}.$$

Consequently, we write

$$\begin{aligned} I\!H_V\left(\boldsymbol{w}_h^{(L)}, \boldsymbol{w}_h^{(A)}, \boldsymbol{n}_B\right) &= \mathbf{P}^+(\boldsymbol{n}_B)\,\boldsymbol{w}_h^{(L)} + \mathbf{P}^-(\boldsymbol{n}_B)\,\boldsymbol{w}_h^{(A)} \\ &= \mathbf{P}^+(\boldsymbol{n}_B)\,\boldsymbol{w}_h^{(L)} + \mathbf{P}_A^-(\boldsymbol{n}_B)\,\boldsymbol{w}_h^{(L)}, \end{aligned} \tag{18}$$

where $\mathbf{P}^+(\boldsymbol{n}_B)$ is defined in the spirit of Eq. (14) with the wave speed $c = c_B$ and

$$\mathbf{P}_A^-(\boldsymbol{n}_B) = \frac{1}{2}\begin{pmatrix} -\frac{\rho_A}{\rho_B}c_A n_1^2 & -\frac{\rho_A}{\rho_B}c_A n_1 n_2 & -n_1 \\ -\frac{\rho_A}{\rho_B}c_A n_1 n_2 & -\frac{\rho_A}{\rho_B}c_A n_2^2 & -n_2 \\ -\frac{\rho_A}{\rho_B}c_A^2 n_1 & -\frac{\rho_A}{\rho_B}c_A^2 n_2 & -c_A \end{pmatrix}.$$

Analogously to the previous approach, we get from Eq. (9)

$$\boldsymbol{w}_h^{(B)} = \left(\frac{\rho_B}{\rho_A}\,w_1^{(R)}, \frac{\rho_B}{\rho_A}\,w_2^{(R)}, w_3^{(R)}\right)^{\mathrm{T}},$$

and we obtain

$$\begin{aligned} I\!H_V\left(\boldsymbol{w}_h^{(R)}, \boldsymbol{w}_h^{(B)}, \boldsymbol{n}_A\right) &= \mathbf{P}^+(\boldsymbol{n}_A)\,\boldsymbol{w}_h^{(R)} + \mathbf{P}^-(\boldsymbol{n}_A)\,\boldsymbol{w}_h^{(B)} \\ &= \mathbf{P}^+(\boldsymbol{n}_A)\,\boldsymbol{w}_h^{(R)} + \mathbf{P}_B^-(\boldsymbol{n}_A)\,\boldsymbol{w}_h^{(R)}, \end{aligned} \tag{19}$$

where $\mathbf{P}^+(\boldsymbol{n}_A)$ has the same form as in Eq. (14) with the wave speed $c = c_A$ and

$$\mathbf{P}_B^-(\boldsymbol{n}_A) = \frac{1}{2}\begin{pmatrix} -\frac{\rho_B}{\rho_A}c_B n_1^2 & -\frac{\rho_B}{\rho_A}c_B n_1 n_2 & -n_1 \\ -\frac{\rho_B}{\rho_A}c_B n_1 n_2 & -\frac{\rho_B}{\rho_A}c_B n_2^2 & -n_2 \\ -\frac{\rho_B}{\rho_A}c_B^2 n_1 & -\frac{\rho_B}{\rho_A}c_B^2 n_2 & -c_B \end{pmatrix}.$$

On the far-filed boundary $\partial\Omega$, which is assumed fixed, we proceed as follows. The setting of boundary conditions for the problem is determined by the fact that the stresses must vanish on this boundary. Moreover, the wave velocities (also momentum) are chosen here in a more sophisticated way to preserve the amount of momentum and to get it away from the whole system as rapidly as possible. Since the domain Ω has a rectangular shape with sides parallel to coordinate axes, this approach leads us to the definition of the following state vector on the boundary as

$$\boldsymbol{w}_h^{(E)} = \left(\sqrt{\left(w_1^{(L)}\right)^2 + \left(w_2^{(L)}\right)^2}\,n_1, \sqrt{\left(w_1^{(L)}\right)^2 + \left(w_2^{(L)}\right)^2}\,n_2, 0\right)^{\mathrm{T}},$$

where the vector $(n_1, n_2)^{\mathrm{T}}$ denotes the unit outer normal to $\partial\Omega$.

Then, for all $\Gamma \in \mathcal{F}_h^B$, we rewrite the numerical flux from Eq. (16) with respect to boundary conditions as

$$I\!H_V\left(\boldsymbol{w}_h^{(L)}, \boldsymbol{w}_h^{(E)}, \boldsymbol{n}_\Gamma\right) = \mathbf{P}^+(\boldsymbol{n})\,\boldsymbol{w}_h^{(L)} + \mathbf{P}^-(\boldsymbol{n})\,\boldsymbol{w}_h^{(E)}, \tag{20}$$

where $\mathbf{P}^+(\boldsymbol{n})$ and $\mathbf{P}^-(\boldsymbol{n})$ are defined with the wave speed $c = c_A$ according to Eqs. (14) and (15), respectively.

3.3 Implicit numerical scheme

Since the semidiscrete scheme (17) represents a system of ordinary differential equations, we employ suitable solvers for the time integration, giving the suitable order of convergence in time with the unconditional stability and no limitations on the length of the time step. The crucial idea is to start from the backward Euler method for time derivative, use an implicit approach in all terms of Eq. (10) except for the nonlinear far-field boundary conditions, which are treated explicitly.

For simplicity, let us construct a partition $0 = t_0 < t_1 < t_2 < t_M = T$ of the time interval $[0, T]$ with a constant time step $\tau = T/M$ and use the approximations $\boldsymbol{w}_h(t_k) \approx \boldsymbol{w}_h^k \in \boldsymbol{S}_{hp}$ for all time instants t_k. Then the resulting implicit scheme reads: for given discrete state $\boldsymbol{w}_h^k \in \boldsymbol{S}_{hp}$ find the new one $\boldsymbol{w}_h^{k+1} \in \boldsymbol{S}_{hp}$ according to the following formula

$$\left(\frac{\boldsymbol{w}_h^{k+1} - \boldsymbol{w}_h^k}{\tau}, \boldsymbol{\varphi}_h \right) + \widehat{b}_h(\boldsymbol{w}_h^{k+1}, \boldsymbol{\varphi}_h) = \widehat{l}_h(\boldsymbol{w}_h^k, \boldsymbol{\varphi}_h) \quad \forall\, \boldsymbol{\varphi}_h \in \boldsymbol{S}_{hp},\ k = 0, 1, \dots \tag{21}$$

with the starting data $\boldsymbol{w}_h^0$, bilinear form $\widehat{b}_h$ and the right-hand side form $\widehat{l}_h$, defined using Eqs. (12), (16) and (18)–(20) as

$$\begin{aligned}
\widehat{b}_h(\boldsymbol{w}_h^{k+1}, \boldsymbol{\varphi}_h) \;=\; & - \sum_{K \in \mathcal{T}_h} \int_K \frac{\partial \boldsymbol{\varphi}_h^{\mathrm{T}}}{\partial x} \mathbf{A}(\boldsymbol{x})\, \boldsymbol{w}_h^{k+1}\, \mathrm{d}\boldsymbol{x} - \sum_{K \in \mathcal{T}_h} \int_K \frac{\partial \boldsymbol{\varphi}_h^{\mathrm{T}}}{\partial y} \mathbf{B}(\boldsymbol{x})\, \boldsymbol{w}_h^{k+1}\, \mathrm{d}\boldsymbol{x} \\
& + \sum_{\Gamma \in \mathcal{F}_h^I} \int_\Gamma [\boldsymbol{\varphi}_h^{\mathrm{T}}] \left(\mathbf{P}^+(\boldsymbol{n})\, \boldsymbol{w}_h^{k+1(L)} + \mathbf{P}^-(\boldsymbol{n})\, \boldsymbol{w}_h^{k+1(R)} \right) \mathrm{d}S \\
& + \sum_{\Gamma \in \mathcal{F}_h^T} \int_\Gamma \boldsymbol{\varphi}_h^{\mathrm{T}(L)} \left(\mathbf{P}^+(\boldsymbol{n}_B) + \mathbf{P}_A^-(\boldsymbol{n}_B) \right) \boldsymbol{w}_h^{k+1(L)}\, \mathrm{d}S \\
& + \sum_{\Gamma \in \mathcal{F}_h^T} \int_\Gamma \boldsymbol{\varphi}_h^{\mathrm{T}(R)} \left(\mathbf{P}^+(\boldsymbol{n}_A) + \mathbf{P}_B^-(\boldsymbol{n}_A) \right) \boldsymbol{w}_h^{k+1(R)}\, \mathrm{d}S \\
& + \sum_{\Gamma \in \mathcal{F}_h^B} \int_\Gamma \boldsymbol{\varphi}_h^{\mathrm{T}(L)}\, \mathbf{P}^+(\boldsymbol{n})\, \boldsymbol{w}_h^{k+1(L)}\, \mathrm{d}S
\end{aligned}$$

and

$$\widehat{l}_h(\boldsymbol{w}_h^k, \boldsymbol{\varphi}_h) = - \sum_{\Gamma \in \mathcal{F}_h^B} \int_\Gamma \boldsymbol{\varphi}_h^{\mathrm{T}(L)}\, \mathbf{P}^-(\boldsymbol{n})\, \boldsymbol{w}_h^{k(E)}\, \mathrm{d}S.$$

Since the problem (3) is linear, the implicit treatment in Eq. (17) also leads to a linear algebraic problem (21) at each time level, which can be further represented in the matrix-vector form.

Next, we rewrite the discrete solution at the time level t_k as a linear combination of basis functions, i.e.

$$\boldsymbol{w}_h^k(\boldsymbol{x}) = \sum_{j=1}^{\mathrm{DOF}} \xi_j^k \cdot \boldsymbol{\varphi}_h^{(j)}(\boldsymbol{x}),\ \boldsymbol{x} \in \Omega, \quad \text{and} \quad \boldsymbol{S}_{hp} = \mathcal{L}\left(\boldsymbol{\varphi}_h^{(1)}, \dots, \boldsymbol{\varphi}_h^{(\mathrm{DOF})} \right),$$

where DOF denotes the number of degrees of freedom (corresponding with the dimension of $\boldsymbol{S}_{hp}$) and $\mathcal{L}$ the linear span, respectively. Now, if we set the vector of

real coefficients $\mathbf{z}^k = \{\xi_j^k\}_{j=1}^{\mathrm{DOF}}$, then, from Eq. (21) we receive the sparse matrix equation

$$(\mathbf{M} + \tau\mathbf{C})\,\mathbf{z}^{k+1} = \mathbf{M}\mathbf{z}^k + \tau\mathbf{f}^k, \tag{22}$$

where the matrix $\mathbf{M}$ is related to the mass matrix, the matrix $\mathbf{C}$ to the form $\widehat{b}_h$ and the vector $\mathbf{f}^k$ represents the right-hand side form $\widehat{l}_h$, respectively.

The system matrix is a composition of particular sparse matrices, where the mass matrix is symmetric and positive definite, and the structure of the matrix $\mathbf{C}$ arises from the physical background of the problem and depends essentially on the numerical flux $I\!H_V$. Using the spectral theory in this upwind scheme (cf. [14]), it can be shown that the matrix $\mathbf{C}$ is non-symmetric and singular, and has indefinite symmetric part, but its entire spectrum lies in the right half of the complex plane. Therefore, one can easily conclude that all time steps $\tau > 0$ always guarantee that the system matrix $\mathbf{M} + \tau\mathbf{C}$ is nonsingular, i.e. zero is not contained in its spectrum.

Consequently, the system matrix has an inverse, which implies the solvability of the algebraic problem (22). Finally, let us mention that the DG solution $\boldsymbol{w}_h^{k+1}$ at each time level is uniquely determined by the solution vector $\mathbf{z}^{k+1}$.

3.4 Limiting procedure

In the elasticity interface problems the discontinuous material parameters ρ and E across certain interfaces imply discontinuities along these interfaces in other physical quantities. In this studied problem such discontinuities are allowed for the momentum and the strain, while the displacement vector and the stress are treated continuously due to interface conditions (7). In numerical solutions they are usually accompanied by nonphysical spurious overshoots and undershoots in the vicinity of these areas with very steep gradients of these solutions.

In order to avoid this undesirable phenomenon, it is necessary to apply a suitable limiting procedure. The idea follows the approach proposed in [4] and is based on a replacement of the solution in the problematic subdomains by its projection into the space of piecewise constant functions. In the rest, the numerical solution remains unchanged.

At first, to identify the elements with possible spurious oscillations in the numerical solution we employ the following discontinuity indicator

$$g(K) = \frac{1}{\mathrm{diam}(K)|K|^{3/4}} \int_{\partial K} [w_{h,3}^k]^2 \,\mathrm{d}S, \quad K \in \mathcal{T}_h, \tag{23}$$

where $\mathrm{diam}(K)$ and $|K|$ denotes the diameter and the area of the element K, respectively. This indicator is based on the stress function (i.e. the third component of $\boldsymbol{w}_h^k$), because this quantity is more suitable for the identification of discontinuities or very steep gradients in the solutions than the strain function. The strain can be a priori discontinuous on interfaces due to the different Young moduli on each subdomain in general, and therefore such indicator could be incorrect.

Secondly, on an arbitrary element K, the projection Π_0 is given by the integral average value

$$\Pi_0(\varphi|_K) = \frac{1}{|K|} \int_K \varphi \,\mathrm{d}x, \quad K \in \mathcal{T}_h,\ \varphi \in L^2(\Omega). \tag{24}$$

Consequently, the updated solution $\widehat{\boldsymbol{w}}_h^k$ is defined via Eqs. (23) and (24) element-wise

$$\widehat{\boldsymbol{w}}_h^k|_K = \begin{cases} \Pi_0\left(\boldsymbol{w}_h^k|_K\right), & \text{if} \quad g(K) > 1, \\ \boldsymbol{w}_h^k|_K, & \text{if} \quad g(K) \leq 1. \end{cases} \tag{25}$$

The resulting scheme equipped with the automatic limiting reads

$$(\mathbf{M} + \tau \mathbf{C})\, \mathbf{z}^{k+1} = \mathbf{M}\widehat{\mathbf{z}}^k + \tau \mathbf{f}^k,$$

where $\widehat{\mathbf{z}}^k$ is a vector of basis coefficients for the modified solution $\widehat{\boldsymbol{w}}_h^k$ from Eq. (25).

Finally, note that the indicator (23) was originally proposed for piecewise linear approximations. However, this limiting procedure works with similar results also for piecewise quadratic and cubic approximations in the studied problem. The higher orders are not considered here, in order to preserve p-quasi-uniformity, i.e. to avoid larger differences in polynomial orders for a set of neighbouring elements.

4. Numerical experiments

Our aim is to demonstrate the behaviour of the aforementioned elastic medium subjected to two different kinds of an external action: (i) the initial impact representing some kind of a mechanical hit with a certain intensity and locality; (ii) the initial stress of a compact support corresponding to some kind of a mechanical loading. From the mathematical point of view the both types of action correspond only to the different choices of initial states $\boldsymbol{w}^0$.

These outer interventions cause a development and propagation of waves, whose amplitudes correspond to extremal values of the displacements $\boldsymbol{u}$, secondly implying the value of stresses σ. The most important observations are especially travelling waves through the interface and the distribution of stresses in its neighbourhood.

The nature of the problem and the form of the system (3) guarantee the direct evaluation of all components of the state vector, i.e. momentum and stress, or deformation velocities and strain derived from them, respectively. However, in some situations it is necessary to compute also the displacement vector $(u_h, v_h)^{\mathrm{T}}$. Calculation of the displacement is therefore determined by the additional solving of a couple of ordinary differential equations (arising from the definition of $\boldsymbol{w}$)

$$\frac{\mathrm{d}u_h}{\mathrm{d}t} = \frac{1}{\rho}\, w_{h,1}(t) \qquad \text{and} \qquad \frac{\mathrm{d}v_h}{\mathrm{d}t} = \frac{1}{\rho}\, w_{h,2}(t), \tag{26}$$

where functions $w_{h,1}(t)$ and $w_{h,2}(t)$ are known only at partition nodes t_k of the time interval $[0, T]$. The solutions u_h^k and v_h^k of the system (26) can be obtained by a suitable time integration. For instance, we can employ an implicit Euler method again as in Eq. (22) and solve Eq. (26) together with the original problem.

Next, we introduce the geometry of a computational domain. For simplicity, we consider the following planar elastic domain Ω with a circular subdomain Ω_B with unit radius, i.e.,

$$\Omega = (0, 10) \times (0, 10), \qquad \Omega_B = \left\{[x, y] \in I\!R^2 : (x-5)^2 + (y-6)^2 < 1\right\}.$$

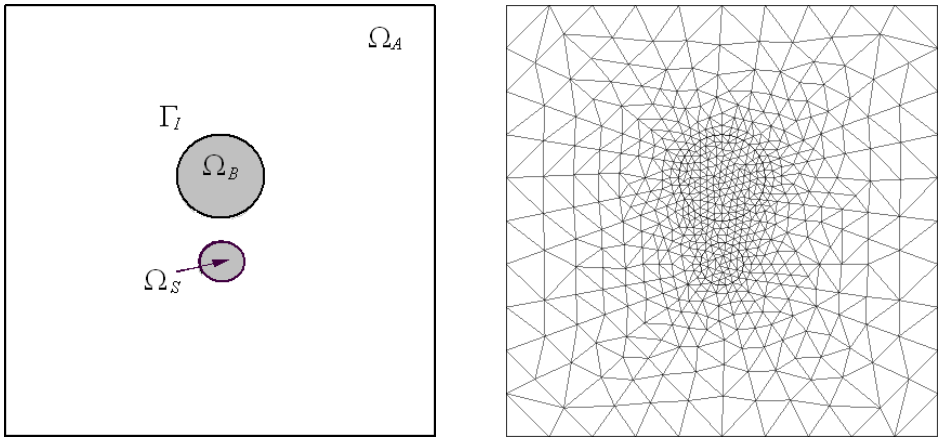

Fig. 2 *Spatial domain – the position of an interface and impact zone Ω_S (left) and the corresponding adaptively refined triangulation with 1128 elements (right).*

Then the second subdomain is constructed as $\Omega_A = \Omega \backslash \overline{\Omega_B}$ and the interface is given by $\Gamma_I = \overline{\Omega_A} \cap \overline{\Omega_B}$, see Fig. 2 (left). The whole triangulation $\mathcal{T}_h$ of a such domain Ω is depicted in Fig. 2 (right) with obvious refinement.

All computations are carried out with an algorithm implemented in the solver Freefem++, see [6], from a mesh generation/adaptation, over the discretization and assembly of a linear algebraic problem to the basic post-processing. In the forthcoming numerical experiments we consider piecewise linear ($p = 1$) discontinuous elements with constant time step $\tau = 0.01$. The computational meshes have approximately 6 000 elements and UMFPACK is used as a sparse solver.

The presented numerical scheme (22) has theoretical order of accuracy $(p + \frac{1}{2}, 1)$ on general grids, i.e. the norm of the error satisfies

$$\left\|\boldsymbol{w}(t_k) - \boldsymbol{w}_h^k\right\| := \sqrt{\sum_{K \in \mathcal{T}_h} \left(\boldsymbol{w}(t_k) - \boldsymbol{w}_h^k, \boldsymbol{w}(t_k) - \boldsymbol{w}_h^k\right)} = \mathcal{O}\left(h^{p+\frac{1}{2}} + \tau\right),$$

for a sufficiently smooth solution $\boldsymbol{w}$ and for all t_k on any interval $[0, T]$, see [7]. Concurrently with this estimate, we also obtain a priori semidiscrete bounds to control the solution on the entire time interval $[0, T]$ by the initial data. As stated in [7], there exists constants C_h and α_h such that

$$\sup_{t \in [0,T]} \left\|\boldsymbol{w}_h(t)\right\|^2 \leq C_h \, e^{\alpha_h T} \left\|\boldsymbol{w}_h(0)\right\|^2.$$

According to the numerical results, this setting of space-time approximations does not lead to a decrease of the accuracy, when an adaptively refined grid is used and the time step is proportional to the wave speed. The significantly large time step can destroy the accuracy as a poor resolution of a propagation of travelling waves, especially in the neighbourhood of interfaces. On the other hand, the order of accuracy with respect to the time coordinate can be increased by using the higher-order scheme, e.g. the Crank-Nicolson method.

4.1 Mechanical hit

First, let us consider the following (dimensionless) parameters of a medium: $\rho_A = 1\,000$, $E_A = 1\,000$, $\rho_B = 1\,000$, $E_B = 16\,000$, subjected to the mechanical hit. Before it, the whole system is in equilibrium, i.e. displacements and stress have zero values. The energy supplied to the system by the initial impact is modeled by non-zero initial velocities given by 2D cylindrically symmetric Gaussian pulse centered at the point $(5, 4)$ with the unit amplitude and variances 0.01 in x and y directions. Here we assume that an initial impact comes from the direction parallel to y-coordinate axis. Thus, the resulting initial state vector is given by

$$\boldsymbol{w}^0(\boldsymbol{x}) = \left(0, \rho(\boldsymbol{x}) \exp\left(-50 \cdot |\boldsymbol{x} - (5,4)|^2\right), 0\right)^{\mathrm{T}}, \quad \boldsymbol{x} \in \Omega.$$

Next, through a series of snapshots, we show in Fig. 3 the development of the DG approximations of stress and strain from the initial zero data up to the final time $T = 3.0$. At the first sight, the isolines of stresses and strains may seen very similar, because the strain can be interpreted as the rescaled stress by the Young modulus. However, in a detailed view of the subdomain Ω_B, one can easily recognize differences between the propagation of stress and strain. It can be stated that the stress propagates through the circular interface Γ_I continuously, see Fig. 3 (left). On the contrary, the isolines of strains are shifted on this interface and therefore are discontinuous, see Fig. 3 (right). This fact secondarily reveals the heterogeneous structure of the elastic medium, arising from parameters $E_A \neq E_B$. These experiments also demonstrate that the corresponding wavefronts of stress propagate faster in region Ω_B than in subdomain Ω_A, which is in a good agreement with parameters of a medium considered, where $c_A < c_B$.

4.2 Mechanical loading

In the second example we consider another scenario, where the elastic medium with parameters $\rho_A = 1\,000$, $E_A = 1\,000$, $\rho_B = 2\,000$, $E_B = 8\,000$ is subjected to the mechanical loading. A balanced system is supplemented by the initial stress of the constant value uniformly distributed on the subdomain $\Omega_S = \{[x, y] \in \mathbb{R}^2 : (x-5)^2 + (y-4)^2 < 0.25\}$, see Fig. 2 (left). Therefore, we take into account

$$\boldsymbol{w}^0(\boldsymbol{x}) = \left(0, 0, 10 \cdot \chi(\overline{\Omega_S})\right)^{\mathrm{T}}, \quad \boldsymbol{x} \in \Omega,$$

where $\chi(\overline{\Omega_S})$ is the characteristic function of the closure $\overline{\Omega_S}$.

In Fig. 4, at the beginning of the whole simulation $t \in [0, 3]$, it is evident that the initial piecewise constant profile of the stress has broken up into different waves preserving the symmetry of the problem setting. Later, one can easily observe the behaviour of wavefronts along the interface, which is characterized by the transmission and reflection of a wave during the transition of heterogeneity. Similarly, as in the previous experiment, the numerical solution satisfies the coupling conditions on the interface with continuous stresses and generally discontinuous strains.

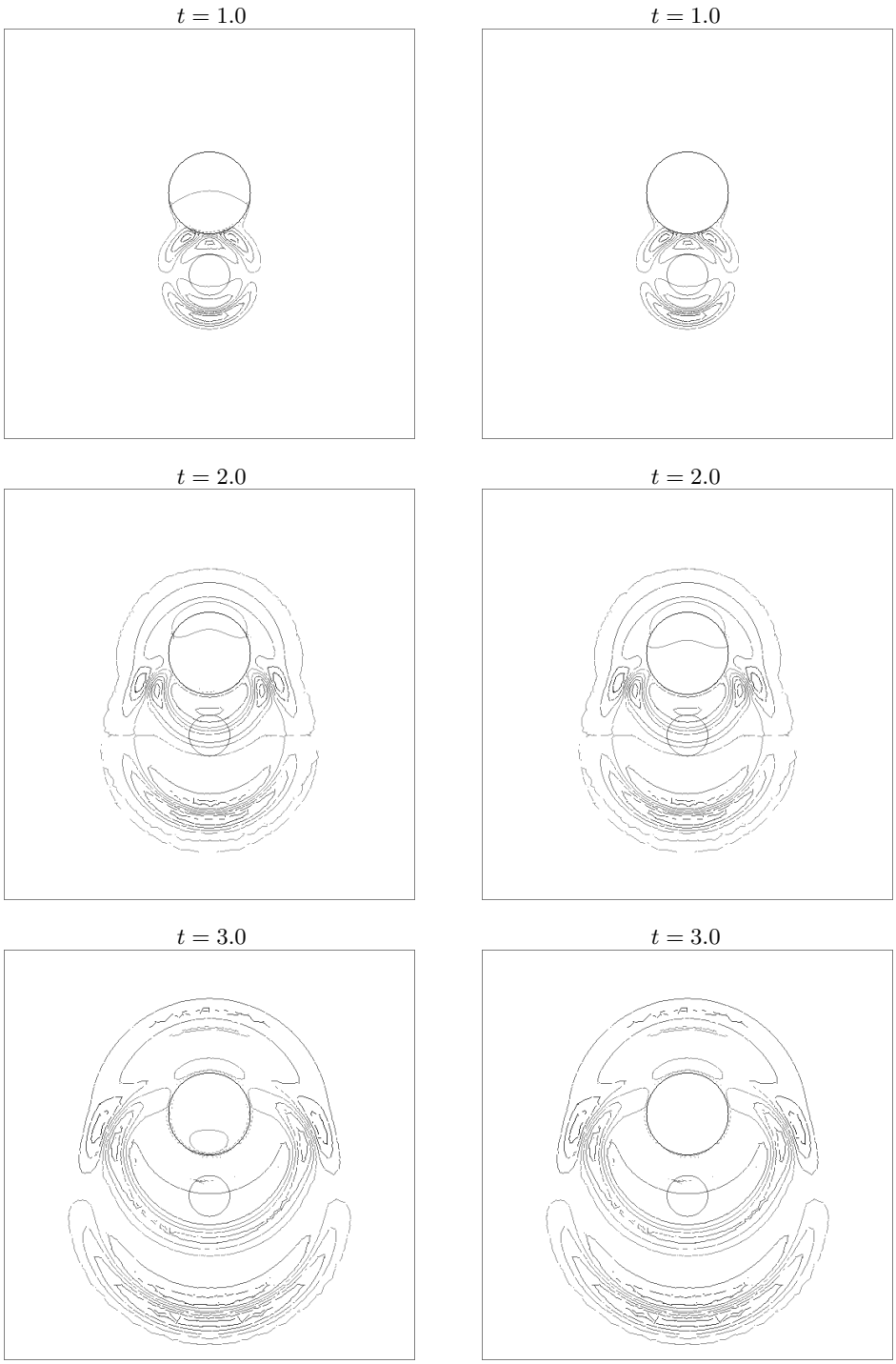

Fig. 3 *Mechanical hit: Development of distribution of approximate stresses (left) and strains (right) in the whole medium captured at monitored time instants.*

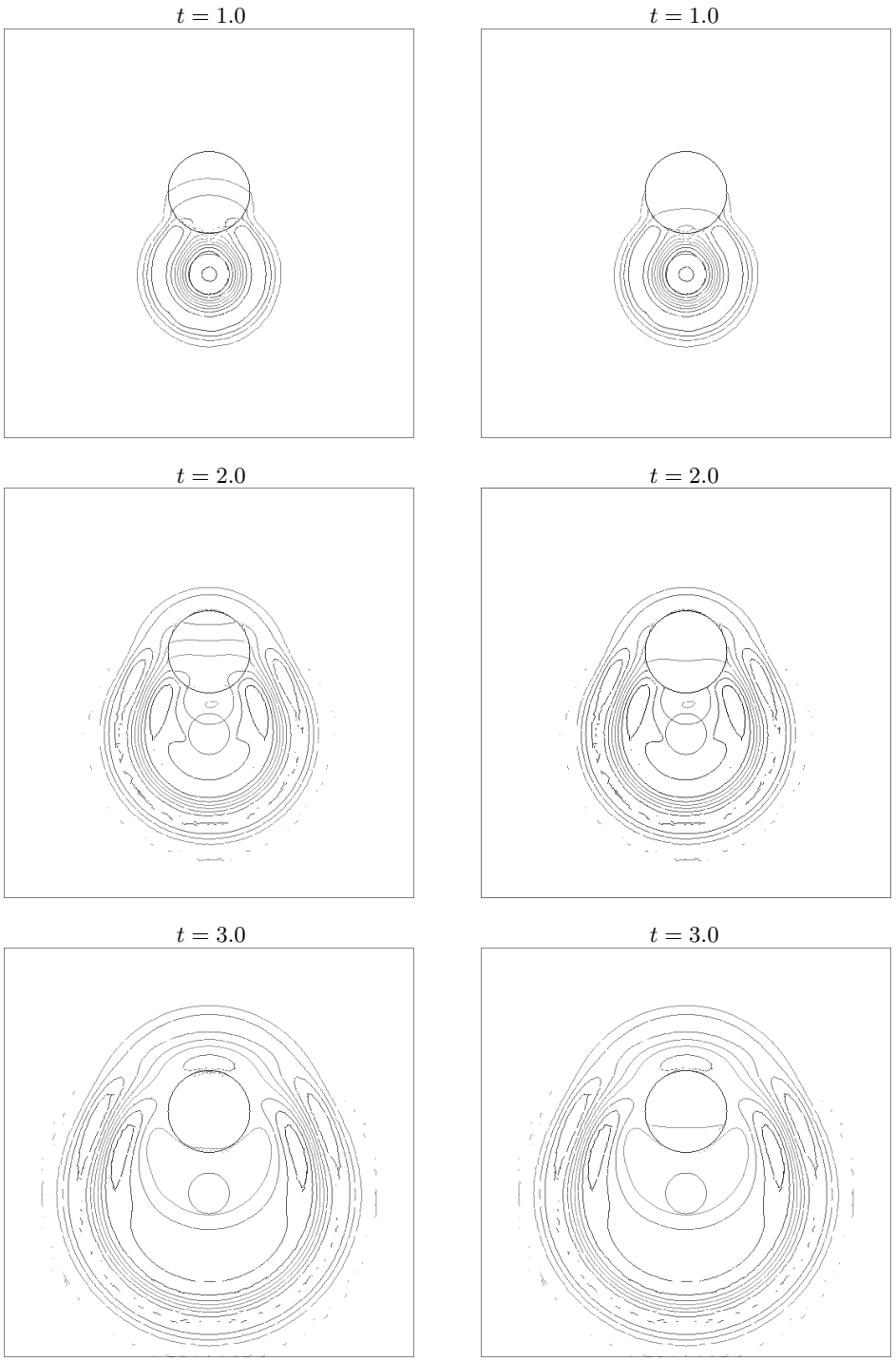

Fig. 4 *Mechanical loading: Development of distribution of approximate stresses (left) and strains (right) in the whole medium captured at monitored time instants.*

5. Concluding remarks

We have presented a DG solver for the treatment of simplified elastic wave equations that arise from the linear elasticity problem and that model a propagation of mechanical waves in the piecewise homogeneous media. We have shown numerically that both elaborated experiments reflect desired results. Therefore the potential of this solver is promising for usage in many disciplines.

In the first place, the sophisticated choice of artificial boundary conditions leading to the elimination of undesired effects on the boundary enables to sufficiently diminish the diameter of the whole computational domain. Secondly, the elastic wave propagation depends also on the shape of the domain Ω_B and its position with respect to the impact zone. In order to simplify this dependency, in this study the interface of a circular shape is chosen and approximated with a sufficiently refined convex polygon. Finally, limiting together with an implicit treatment in interface conditions clearly resolve the discontinuities in each component of the solution.

Further, using the inverse approach to the problem solution, the structure of the material can be revealed from the real experiments and this can be also applied in the field of biological materials and biomechanics, especially for the determination of load limits of human body in case of a traffic accident, see [13]. Moreover, it can be useful for the design of passive safety elements of the vehicle, cf. [9].

The presented continuous model has also its limitations consisting in the simple form of the stress tensor, which takes into account only a propagation of longitudinal waves in the medium with piecewise constant parameters. Possible ways to extend this model consist in the introduction of an additional material parameter corresponding to the propagation of transverse waves together with the assumption of heterogeneity of the medium, which can be objects of interest for the future work.

Acknowledgement

This work was partly supported by the Czech Science Foundation under project 16-09541S, by SGS Project 'Modern numerical methods III' financed by TU Liberec, and by the institutional funding for long-term strategic development of the University of West Bohemia provided by the Ministry of Education of the Czech Republic. The support is greatly acknowledged.

References

[1] CHANG Y. The adaptive immersed interface finite element method for elasticity interface problems. *Journal of Computational Mathematics*. 2012, 30(6), pp. 629–642, doi: 10.4208/jcm.1203-m3869.

[2] COCKBURN B., KARNIADAKIS G.E., SHU C.-W. *Discontinuous Galerkin Methods*. Berlin, Germany: Springer, 2000, doi: 10.1007/978-3-642-59721-3.

[3] DOLEJŠÍ V., FEISTAUER M. *Discontinuous Galerkin Method – Analysis and Applications to Compressible Flow*. Heidelberg, Germany: Springer, 2015. doi: 10.1007/978-3-319-19267-3.

[4] DOLEJŠÍ V., FEISTAUER M., SCHWAB C. On some aspects of the discontinuous Galerkin finite element method for conservation laws. *Mathematics and Computers in Simulation*. 2003, 61(3-6), pp. 333–346, doi: 10.1016/S0378-4754(02)00087-3.

[5] GREEN A.E., ZERNA W. *Theoretical Elasticity*. London, UK: Oxford University Press, 1968.

[6] HECHT F. New development in FreeFem++. *Journal of Numerical Mathematics*. 2012, 20(3-4), pp. 251–265, doi: 10.1515/jnum-2012-0013.

[7] HESTHAVEN J.S., WARBURTON T. *Nodal Discontinuous Galerkin Methods – Algorithms, Analysis, and Applications*. New York: Springer-Verlag, 2008. doi: 10.1007/978-0-387-72067-8.

[8] HOZMAN J., BRADÁČ J., KOVANDA J. Neural tissue response to impact - numerical study of wave propagation at level of neural cells. *Neural Network World*. 2014, 24(2), pp. 157–176, doi: 10.14311/NNW.2014.24.010.

[9] KOVANDA J., RIVA R. *Vehicle human interaction. Passive safety of vehicle*. Milano, Italy: Spiegel, 1998.

[10] LANDAU L.D., LIFSHITZ E.M. *Theory of Elasticity*. Oxford, UK: Pergamon Press, 1975.

[11] MARTINS-COSTA M.L., DA GAMA R.M.S. Simulation of wave propagation in a piecewise homogeneous elastic rod. *International Journal of Structural Changes in Solids - Mechanics and Applications*. 2011, 3(2), pp. 47–54 [viewed 2015-11-14]. Available from: https://journals.tdl.org/ijscs/index.php/ijscs/article/view/2409/2084

[12] RIVIÈRE B. *Discontinuous Galerkin Methods for Solving Elliptic and Parabolic Equations: Theory and Implementation*. Philadelphia, PA: SIAM, 2008, doi: 10.1137/1.9780898717440.

[13] SCHMITT K.-U., NIEDERER P.F., MUSER M.H., WALZ F. *Trauma Biomechanics. Accidental Injury in Traffic and Sports*. Heidelberg, Germany: Springer, 2010, doi: 10.1007/978-3-642-03713-9.

[14] VABISHCHEVICH P.N. SM stability for time-dependent problems. *Numerical Methods and Applications: 7th International Conference, NMA 2010*. Heidelberg, Germany: Springer, 2011, pp. 29–40, doi: 10.1007/978-3-642-18466-6_3.

[15] WANG B., XIA K., WEI G.W. Matched interface and boundary method for elasticity interface problems. *Journal of Computational and Applied Mathematics*. 2015, 285, pp. 29–225, doi: 10.1016/j.cam.2015.02.005.